ARTICLE

P-doped Ru-Pt Alloy Catalyst Toward High Performance Alkaline Hydrogen Evolution Reaction

Rong-Qin Huang [a], Wei-Ping Liao [b], Meng-Xuan Yan [b], Shi Liu [a], Yuan-Ming Li [a], Xiong-Wu Kang [a,*]

[a] Guangdong Huihydrogen Energy Technology Co., Ltd, Guangzhou, 510000, China
[b] Jiangmen Power Supply Bureau of Guangdong Power Grid Co., Ltd, Jiangmen, 529000, China

Abstract

Electrocatalytic water splitting represents grand promise for hydrogen fuel in modern energy equipment, and the design and fabrication of higher performance catalysts are at the central. Herein, we report the sequential phosphorus (P)-doping into ruthenium (Ru) nanoparticles (Ru-P/C) by thermal annealing of Ru nanoparticles in phosphine (PH_3) atmosphere and deposition of extremely low concentration of platinum (Pt) to obtain P-doped Ru-Pt alloy catalyst supported on carbon nanotubes (CNTs), which is denoted as (Ru-P)#Pt/C. The data by X-ray diffraction spectroscopy and transmission electron microscopy show that the Ru nanoparticles existed in the form of hexagonal close-packed (hcp) phase with low crystallinity. The results by high-resolution X-ray photoelectron spectroscopy indicate that Ru was mainly in metallic state, and Pt was slightly and positively charged, ascribing to the bonding with P atoms. This indicates that the highly diluted Pt atoms may be dispersed on the surface of Ru nanoparticles through Ru-P-Pt bonds. Accordingly, the as-prepared (Ru-P)#Pt/C alloy catalysts displayed excellent alkaline hydrogen evolution activity, revealing only 17 mV vs. RHE at a current density of 10 $mA \cdot cm^{-2}$ and a Tafel slope value of 27 $mV \cdot dec^{-1}$, superior to those of the controlled samples Ru-P/C and trace amount of Pt loaded P-doped CNTs (Pt/C-P). Density functional theory (DFT) calculation suggests that P-doping into Ru can enhance the adsorption of water molecules and the activation for water splitting, while the Pt site on Ru-Pt alloy can behave as the hydrogen desorption site. Thus, the superior performance of (Ru-P)#Pt/C alloy catalyst might be attributed to the synergistic effect of P-doped Ru sites and Pt sites, which significantly improves the alkaline hydrogen evolution reaction kinetics.

Keywords: Ru-Pt alloy; Phosphorus-doping; Synergistic effect; Dual active sites; Water splitting

1. Introduction

Electrochemical water splitting driven by renewable energy can achieve the conversion of electric energy to chemical energy of hydrogen, rendering the sustainable hydrogen economy possible [1]. In general, hydrogen evolution reaction (HER) in an acidic electrolyte proceeds through Tafel step by recombination of adsorbed H atoms on the catalyst surface derived from the direct reduction of H^+ in the electrolyte [2]. However, alkaline HER involves water splitting and subsequent evolution of H_2 molecules through either Tafel or Heyrovsky step [3], which is two orders of magnitude slower than acidic HER. Thus, the design of alkaline HER catalysts is more challenging than that of acidic HER catalysts [4]. Since alkaline HER can be performed without using the expensive polymer electrolyte and has been applied in large scale in industry, it is, therefore, desirable to develop low cost and high performance catalysts for alkaline HER [5].

Alloy catalysts have been emerging as a novel designing concept for high performance catalysts and have been applied extensively [6,7]. Alloy catalysts can be prepared by dispersing very small amount of one kind of metal atoms onto the surface of another kind of metal nanoparticles, which can modulate the atomic and electronic structures of the metal nanoparticles, and further the reaction

Received 8 March 2022; Received in revised form 22 March 2022; Accepted 5 April 2022
Available online 7 April 2022

* Corresponding author, Xiong-Wu Kang, Tel: (86-20)39381206, E-mail address: esxkang@scut.edu.cn.

https://doi.org/10.13208/j.electrochem.2203081

intermediates of the reactions and beyond. In recent years, ruthenium (Ru)-based alloys [8,9], due to the extremely high utilization of precious metal and high selectivity toward the specific reactions, have been playing significant roles in heterogeneous catalysis.

Most importantly, Ru is more active for water activation and dissociation, and thus, shows higher promise for alkaline HER than platinum (Pt), due to the less filled *d*-orbital and stronger adsorption to water molecules [10]. However, too strong adsorptions of H and OH upon water splitting on Ru catalysts hinder the desorption of H_2 molecules in Tafel step. Thus, it is desirable to introduce active sites for the desorption of H_2 molecules in Ru-based catalysts for the design of the high-performance electrocatalyst toward alkaline HER. Ru-based alloy catalysts could be prepared by dispersing another metal or nonmetal atoms onto the Ru nanoparticles surface [11], and the electronic structure of the dispersed metal atoms could be well modulated to enhance the catalytic activity and stability of the entire catalysts through the strong metal-support interaction.

Therefore, constructing Ru-based alloy catalysts is a novel pathway for achieving extraordinary alkaline HER catalysts. In this work, we developed a method for fabrication of P-doped Ru-Pt alloy catalysts, denoted as (Ru-P)#Pt/C, which exhibits excellent alkaline HER performance, ascribing to the synergistic effect of P-doped Ru as the excellent water splitting site and Pt atoms as the H_2 desorption site. This work highlights the importance of the P-doping in modulating the electronic structure of Ru metals and the promise of the Ru-Pt alloy catalyst as high performance electrocatalysts for water splitting and beyond.

2. Experimental section

2.1. Materials

Ruthenium trichloride ($RuCl_3$, 99%), chloroplatinic acid hexahydrate ($H_2PtCl_6\cdot 6H_2O$) and sodium borohydride ($NaBH_4$) were obtained from Energy Chemicals. Multi-walled carbon nanotubes (CNTs, >97%), commercial platinum catalyst supported on carbon nanoparticles (Pt/C, 10 wt%) were received from Alfa Aesar. Ethanol (CH_3CH_2OH, 99%), sodium hypophosphite (NaH_2PO_2) and sodium hydroxide (NaOH, 96%) were purchased from Sinopharm Chemical Reagent Co. Ltd. and used directly.

2.2. Syntheses of Ru-P/C, Pt/C-P and (Ru-P)#Pt/C

Ruthenium nanoparticles supported on CNTs were synthesized by an ethanol reduction method. Briefly, 83 mg $RuCl_3$ was dispersed in 100 mL ethanol in a 25 mL flask and refluxed at 110 °C for 1 h in an oil bath under magnetic stirring, into which 200 mg CNTs solution dispersed in ethanol were injected. When the temperature of the solution restabilized at 110 °C, the preprepared 6 mL NaOH solution (0.2 $mol\cdot L^{-1}$) in ethanol was added in one shot. The reaction solution was further stirred at 110 °C for 2 h. Then, additional 0.2 $mol\cdot L^{-1}$ NaOH was added into the reaction flask and refluxed for another 30 min for complete reduction of Ru^{3+} species. The products were precipitated by centrifugation, dried in a vacuum oven overnight and annealed under a mixed H_2/Ar atmosphere at 450 °C for 1 h in a tube furnace, the obtained sample was denoted as Ru/C.

1 g NaH_2PO_2 and 20 mg Ru/C were placed in a tube furnace in the upstream and downstream, respectively, and annealed at 400 °C for 3 h at a ramp rate of 3 $°C\cdot min^{-1}$. The obtained sample was denoted as Ru-P/C. The deposition of diluted Pt atoms on Ru-P/C NPs was finished by following a reported procedure. First, 20 mg Ru-P/C was dispersed in 40 mL ethanol/water mixed solution with a volumetric ratio of 1:1. Then 25 μL 50 $mmol\cdot L^{-1}$ $H_2PtCl_6\cdot 6H_2O$ aqueous solution was added into the above solution dropwise under magnetic stirring. When cooling to 0 °C in an ice bath for 1 h, 1.6 mL 50 $mmol\cdot L^{-1}$ $NaBH_4$ was dissolved in DI water (cooled to 0 °C), injected into the above solution and the reaction last for 1 h. The product was collected by centrifugation and dried in a vacuum oven at 60 °C overnight. The obtained product is labeled as (Ru-P)#Pt/C. As the controlled experiment, the pristine CNTs without adding Ru nanoparticles were equally doped with phosphorus and deposited with Pt atoms by following the same process described as above and the obtained sample is denoted as Pt/C-P.

2.3. Characterizations

The surface morphologies were investigated by high-resolution transmission electron microscopy (HETEM) on JEOL 2100F. The X-ray diffraction (XRD) measurements were performed on a Bruker D8 Advance powder X-ray diffractometer using a Cu-K_α source ($\lambda = 0.154059$ nm at a scan rate of $10^\circ\cdot min^{-1}$). The X-ray photoelectron spectroscopic (XPS) study was performed on an ESCALAB-250Xi X-ray photoelectron spectrometer with an Mg K_α source.

2.4. Electrochemical measurements

The alkaline HER performance of the catalysts was examined on an electrochemical workstation (CH Instrument 760E) in a conventional three-electrode

setup in 1.0 mol·L^{-1} KOH aqueous solution. The Ag/AgCl electrode and a graphite rod were used as the reference and counter electrodes, respectively.

The working electrode was prepared by following the procedures below. 5 mg·mL^{-1} of the catalyst ink was firstly prepared by dispersing 5 mg (Ru-P)#Pt/C catalyst into 1 mL of mixed ultrapure water, isopropanol and Nafion, with a volumetric ratio of 750 μL:250 μL:20 μL by sonication. Before the deposition of the catalyst ink, the glassy carbon electrode (GCE) was cleaned by a sequential sonication in sulfuric acid, nitric acid and DI water for 20 min each. Then 20 μL of the catalyst ink was cast on the GCE dropwise, dried naturally in air and used as the working electrode. Electrochemical measurements were conducted on a CHI 750E electrochemical workstation. All the potentials reported in this work were converted to the reversible hydrogen electrode (RHE).

To remove the dissolved oxygen, the electrolyte was purified with N_2 bubble for 30 min before each test. The final potential was calibrated to the reversible hydrogen electrode (RHE) according to the following equation: $E(\text{RHE}) = E(\text{Ag/AgCl}) + 0.197\ \text{V} + 0.059 \times \text{pH}$. Linear sweep voltammetric (LSV) tests were carried out to examine the electrochemical activity with a scan rate of 1 mV·s^{-1}. The values of Tafel slopes were obtained based on the LSV plots. Electrochemical impedance spectra (EIS) were recorded with an AC amplitude of 10 mV. The frequency ranged from 10 kHz to 0.1 Hz, and the polarization voltage was −0.35 V versus SCE.

2.5. Density functional theory (DFT) calculations

The DFT calculations are performed on the CASTEP module in Material Studio 8.0. The electron exchange and correlation are treated by Perdew-Burke-Ernzerhof (PBE) of the generalized gradient approximation (GGA). The interaction between the valence electrons and ionic core is described by the ultrasoft pseudopotentials (USP). The wave function of the valence electronic states is expanded on the plane-wave basis and the energy cutoff of 450 eV is set. Broyden Fletcher Goldfarb Shanno (BFGS) geometry optimization method is used to find the lowest energy structure. The k-point is set to 3 × 3 × 1 based on Monkhorst-Pack method for the Brillouin zone sampling of unit cell and surface, respectively. A vacuum layer is built with the thickness of 15 Å to ensure the negligible interaction along Z axis. The convergence standard for total energy, maximum force, maximum stress, maximum displacement, self-consistent field (SCF) are 1.0 × 10^{-5} eV·atom^{-1}, 0.03 eV·Å^{-1}, 0.05 GPa, 0.001 Å, and 1 × 10^{-6} eV·atom^{-1}, respectively. The unit cell of hcp Ru (101) is optimized, and the optimized lattice parameters are $a = b = 2.719$ Å and $c = 4.284$ Å.

3. Results and discussion

Fig. 1a displays the TEM image of (Ru-P)#Pt/C. The diameter of the Ru nanoparticles was about 8.2 nm, and the Ru nanoparticles were well distributed on CNTs. The interplanar distances from the HRTEM image (Fig. 1b) were 2.34, 2.14 and 2.05 Å, which are ascribed to the Ru hexagonal close-packed (hcp) (100), (001) and (101), respectively. No Pt nanoparticles were observed in TEM image, indicating that the trace amount of Pt atoms might be dispersed on the Ru nanoparticles and the dilute alloy might be formed [12].

Fig. 2 shows the XRD patterns of CNTs, Ru/CNTs, Ru-P/C and (Ru-P)#Pt/C. The peaks at 42.1°

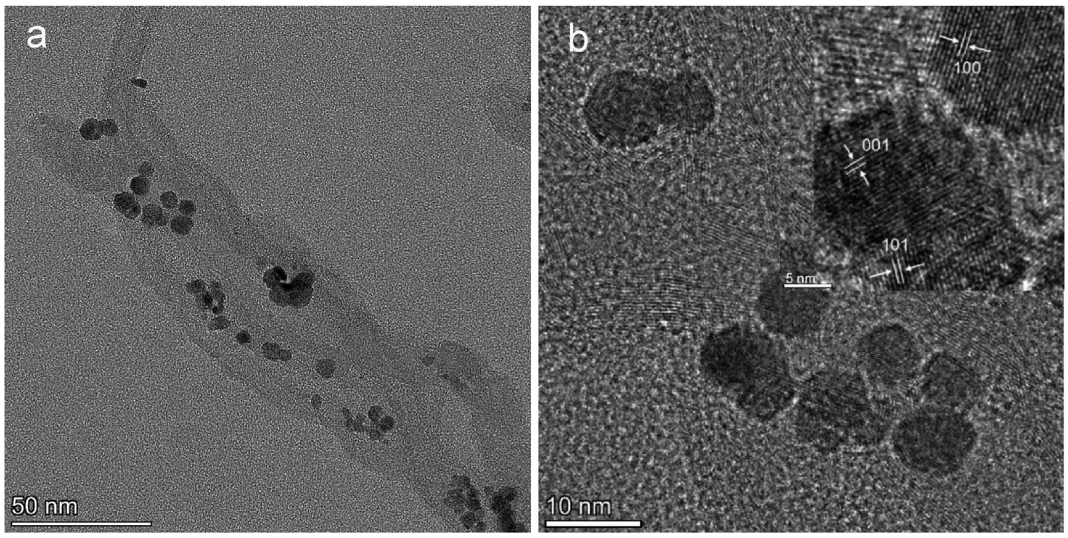

Fig. 1. (a) TEM and (b) HRTEM images of the (Ru-P)#Pt/C catalyst.

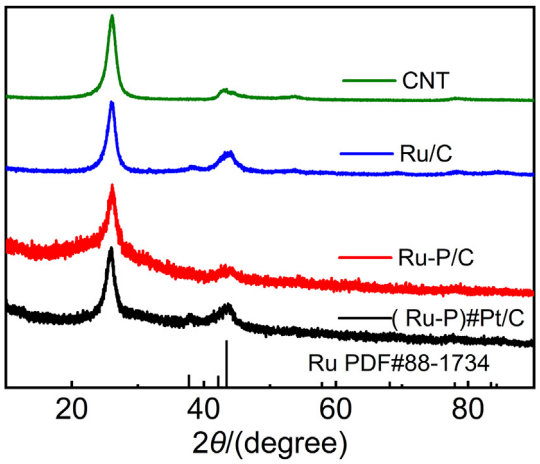

Fig. 2. XRD patterns of the CNTs, Ru/CNTs, Ru-P/C and (Ru-P)#Pt/C catalysts.

and 43.4° indexed to Ru hcp (002) and (101), which overlap with the peaks of CNTs, while the tiny peaks at 37.7° observed for Ru/C and (Ru-P)#Pt/C were exclusively ascribed to Ru hcp (100) facet. For (Ru-P)#Pt/C, no peaks of Pt nanoparticles were observed in the XRD patterns, indicating that Pt atoms may be dispersed on the surface of Ru nanoparticles [12].

The XPS technique was used to characterize the oxidation states of Pt, Ru and P in the samples. Fig. 3a shows the XPS full survey information for Ru-P/C and (Ru-P)#Pt/C, where all Pt, Ru, and P elements were presented, indicating that Pt and P were successfully doped into the Ru nanoparticles. It is derived that the atomic ratio of Pt to Ru in (Ru-P)#Pt/C was less than 14.4% (Table 1), which may result in the atomic dispersion of Pt on the surface of P-doped Ru nanoparticles [12].

Fig. 3b shows high resolution XPS spectrum of P 2*p* for Ru-P/C and (Ru-P)#Pt/C, and the binding energy of P 2*p* was determined to be 133.1 eV, higher than that of Ru-P or Pt-P (129.5 eV). This is mainly ascribed to the C-P/O-P bonding [13], indicating that P is mainly doped into the CNTs, and only the minimum amount of P was doped into the Ru surface and behaved as the active site on the Ru nanoparticles surface for caption of Pt and formation of Ru-P-Pt.

Fig. 3c displays the high resolution XPS spectra of Ru 3*d* and C 1*s* for Ru-P/C and (Ru-P)#Pt/C. The deconvolution indicates the presences of Ru $3d_{5/2}$ and Ru $3d_{3/2}$ at 280.4 and 284.5 eV, which are in the metallic state [12]. The chemical states of Ru element on the surface of Ru nanoparticles did not

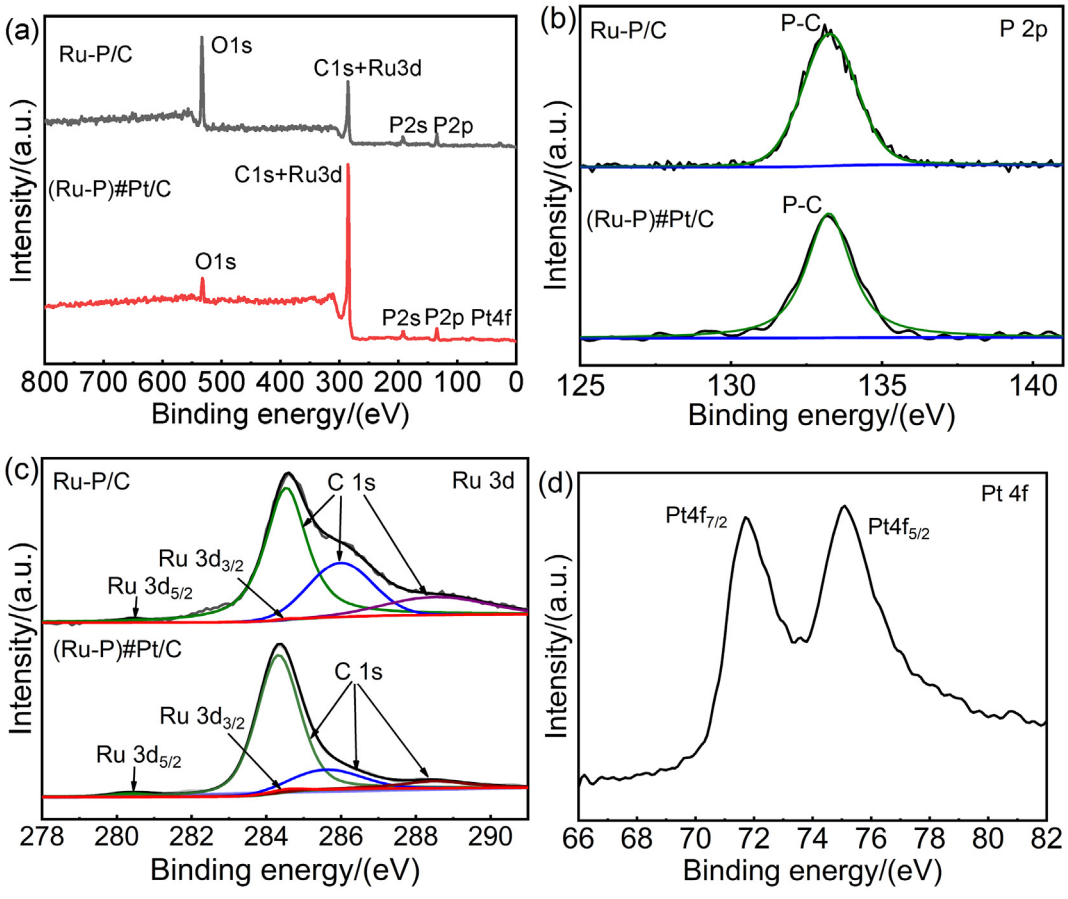

Fig. 3. XPS spectra of the Ru-P/C and (Ru-P)#Pt/C: (a) survey scan curves; (b) P 2p; (c) C 1s and Ru 3d; (d) Pt 4f.

Table 1. Elemental ratios of Ru-P/C and (Ru-P)@Pt from XPS.

Sample	Ru (%)	Pt (%)	P (%)
Ru-P/C	5.32	/	7.55
(Ru-P)#Pt/C	5.23	0.76	7.46

change significantly before and after Pt atom doping. Fig. 3d shows the high resolution XPS of Pt 4*f* for (Ru-P)#Pt/C. The Pt $4f_{7/2}$ and Pt $4f_{5/2}$ were observed at 71.7 and 75.1 eV, respectively, which are positively shifted by 0.7 eV relative to metallic Pt (71.0 eV), but much lower than that of Pt^{2+} (73.2 eV) [14], suggesting that Pt in (Ru-P)#Pt/C possesses a slightly oxidized state, which is attributed to the bonding interaction of Pt atoms with P atoms on the surface of Ru nanoparticles.

Finally, the alkaline HER activity and stability of the (Ru-P)#Pt/C catalyst were examined in 1 mol·L^{-1} KOH, and are compared with those of the Pt/C-P, Pt/C, Ru/C and Ru-P/C catalysts, as shown in Fig. 4. Fig. 4a shows the LSV scans, and the overpotential at a current density of 10 mA·cm^{-2} (η_{10}) was determined to be only 17 mV vs. RHE, much lower than those of the Pt/C (35 mV vs. RHE), Ru/C (63 mV vs. RHE), Pt/C-P (113 mV vs. RHE) and Ru-P/C catalysts (38 mV vs. RHE). By comparing with the poor HER performance of Pt/C-P, the impact of P doping into CNTs and the dispersed Pt atoms on C−P site of CNTs could be ruled out for the excellent HER performance of (Ru-P)#Pt/C. Thus, it is concluded that the co-doping of P and Pt into Ru nanoparticles is indispensable for achieving excellent alkaline HER performance. The introductions of Pt and Ru forms dual active sites, and the synergistic effect between the active sites improved the catalytic activity of HER [12]. Moreover, (Ru-P)#Pt/C outperformed other advanced alkaline-efficient electrocatalysts reported in the literature, as shown in Table 2.

Tafel slope is also an important parameter to evaluate the rate-determining step (RDS). The Tafel slope value of (Ru-P)#Pt/C was 27 mV·dec^{-1} (Fig. 4b), which was lower than those of Pt/C (53 mV·dec^{-1}), Ru/C (66 mV·dec^{-1}), Pt/C−P (128 mV·dec^{-1}) and Ru-P/C (62 mV·dec^{-1}). This means that the HER process is dominated by Tafel step only for (Ru-P)#Pt/C, while Heyrovsky step for Pt/C, Ru/C and Ru-P/C, and Volmer step for Pt/C-P. The turnover frequency (TOF), beyond the overpotential at 10 mA·cm^{-2}, is related to the number of H_2 molecules evolved per second per active site, which is the most important figure of merit to evaluate the intrinsic activity of an

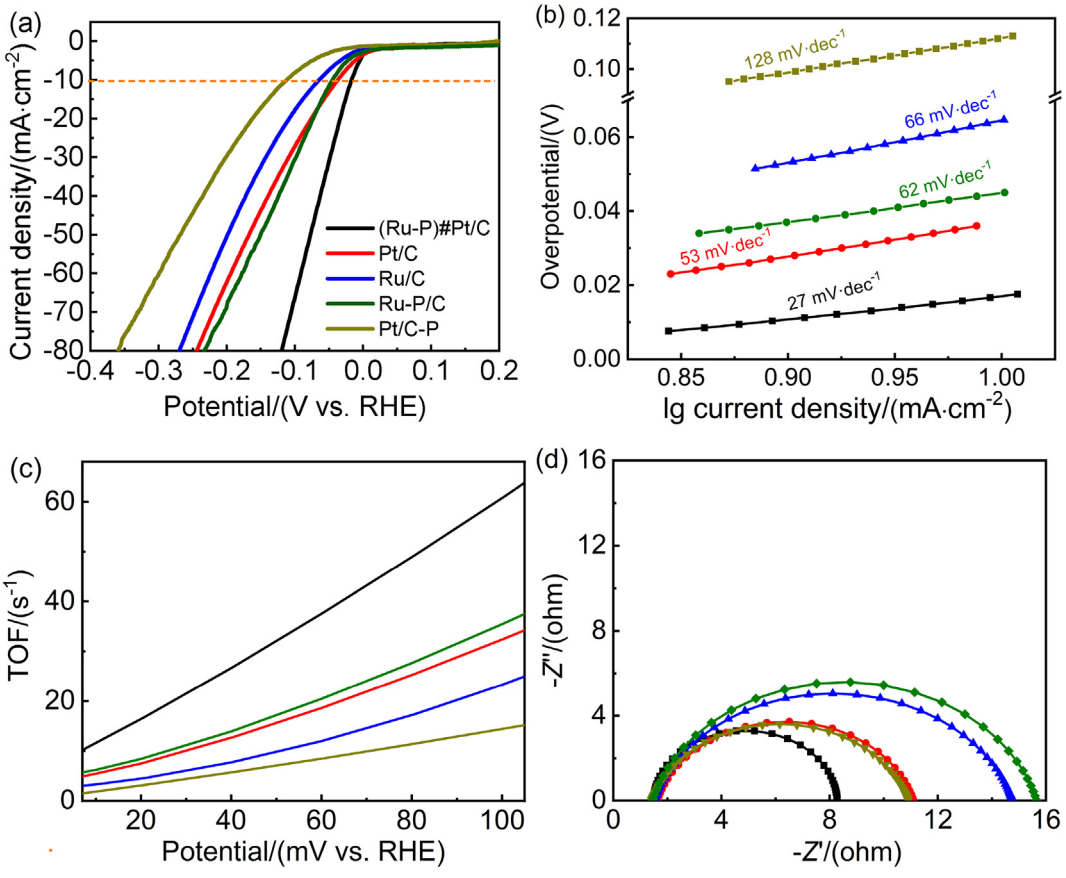

Fig. 4. Electrochemical HER measurements of Pt/C-P, Pt/C, Ru/C, Ru-P/C and (Ru-P)#Pt/C: (a) Linear sweep polarization curves, (b) Tafel slopes, (c) TOF values calculated and (d) Nyquist plots.

Table 2. HER performances of (Ru-P)#Pt/C and previously reported electrocatalysts.

Catalyst	Electrolyte	η10 (mV)	Durability	Reference
(Ru-P)#Pt/C	1.0 mol·L^{-1} KOH	17	24 h	This work
Ru-P/C	1.0 mol·L^{-1} KOH	38		This work
(Ru-N)	1.0 mol·L^{-1} KOH	34.9		[12]
(Ru-N)@Pt	1.0 mol·L^{-1} KOH	15	58 h	[12]
Ru-Pt	1.0 mol·L^{-1} KOH	41		[12]
Pt_3Ni	0.1 mol·L^{-1} KOH	65 (η5)	–	[15]
Pt-Ni(N)	1.0 mol·L^{-1} KOH	13	10 h	[16]
Pt-Ni ASs	1.0 mol·L^{-1} KOH	27.7	10,000 cycles	[17]
Pd-Pt	1.0 mol·L^{-1} KOH	70	2 h	[18]
Ru@C2N	1.0 mol·L^{-1} KOH	17	10,000 cycles	[9]
PtNi-O/C	1.0 mol·L^{-1} KOH	39.8	10 h	[19]
Hcp Pt-Ni	0.1 mol·L^{-1} KOH	65	1 h	[20]
Ru-Ni SNs	0.1 mol·L^{-1} KOH	42.7	–	[21]
PtRu@RFCS	0.5 mol·L^{-1} H_2SO_4	19.5	–	[22]
Ni@Ni_2P-Ru HNRs	1.0 mol·L^{-1} KOH	31	1000 cycles	[8]

electrocatalyst [23]. The TOF value of (Ru-P)#Pt/C at an overpotential of 100 mV vs. RHE was 60.4 s^{-1}, which is much higher than those of Ru/C (23.3 s^{-1}), Ru-P/C (36.5 s^{-1}), Pt/C−P (16.1 s^{-1}) and Pt/C (35.5 s^{-1}) catalysts, indicating that the synergistic doping of P and atomic Pt into Ru nanoparticles can indeed facilitate the intrinsic HER performance in alkaline media.

The electrochemical performances of alkaline HER on Ru/C, Ru-P/C, Pt-P/C and Pt/C, (Ru-P)#Pt/C were further investigated by EIS spectroscopy. The depressed semicircle is attributed to the microscopic roughness of the catalyst film, which induces an inhomogeneous distribution of the solution resistance and the double layer capacitance (Fig. 4d). Besides, the radius of the semicircle reflects the resistance of the charge transfer at the catalyst/electrolyte interface (R_{ct}), where (Ru-P)#Pt/C achieved the lowest R_{ct}, indicating the highest rate of electron transport.

The durability of (Ru-P)#Pt/C sample was assessed by using chronopotentiometry (Fig. 5a) for 24 h and further by LSV scans (Fig. 5b), which retained almost 95% of the current density in LSV after the chronopotentiometric test, indicating its excellent stability in alkaline environment. The slight increase of the η_{10} and reduce of the current density in LSV curves are usually caused by the aggregation of the metal nanoparticles and the reduced surface area. The doping of nonmetal P into Ru nanoparticles may significantly increase the robustness of the Ru nanoparticles against the aggregation and the durability of the catalysts in electrolysis.

The impact of P-doping and formation of Ru-Pt alloy on the kinetics of water splitting and hydrogen evolution are further evaluated by DFT calculation based on Ru (101) and (Ru-P)#Pt (101) model, with the latter model built by doping P atoms into the interstitial site of Ru (101) and replacing partial surface Ru by Pt atoms (Fig. 6). The adsorption configuration of H_2O* and the splitting products of *OH and *H are shown in Fig. 6 and the adsorption energies of the reaction species are listed in Table 3. It is observed that the adsorption energy of water molecule is enhanced by 170 eV on Ru site of (Ru-P)#Pt (101) surface relative to the Ru surface, indicating the enhanced activation of water molecule upon P-doping and the promoted water dissociation in Volmer step [24]. Meanwhile, the adsorption energy of *H atoms on Pt site of (Ru-P)#Pt is 0.4 eV lower than that on Ru surface, which enables the fast

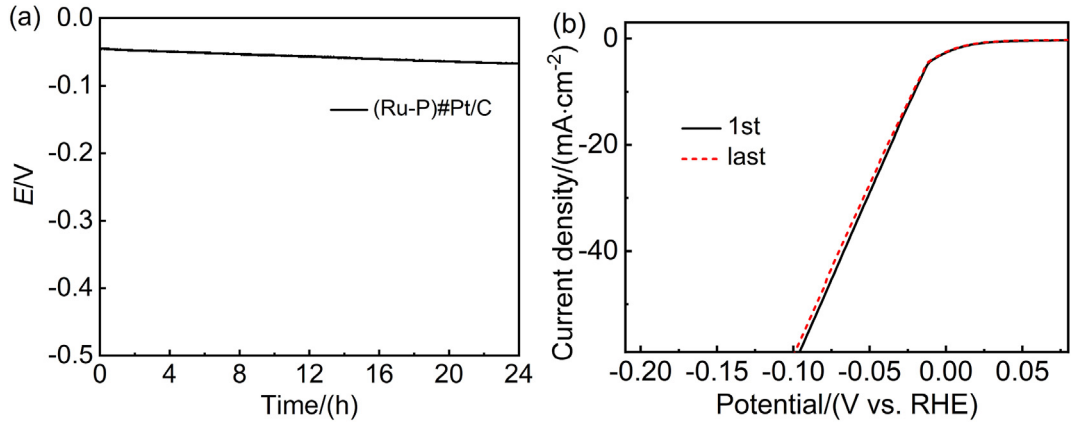

Fig. 5. Chronopotentiometric measurement at 10 mA·cm^{-2} (a) and polarization (b) curves for (Ru-N)#Pt/C.

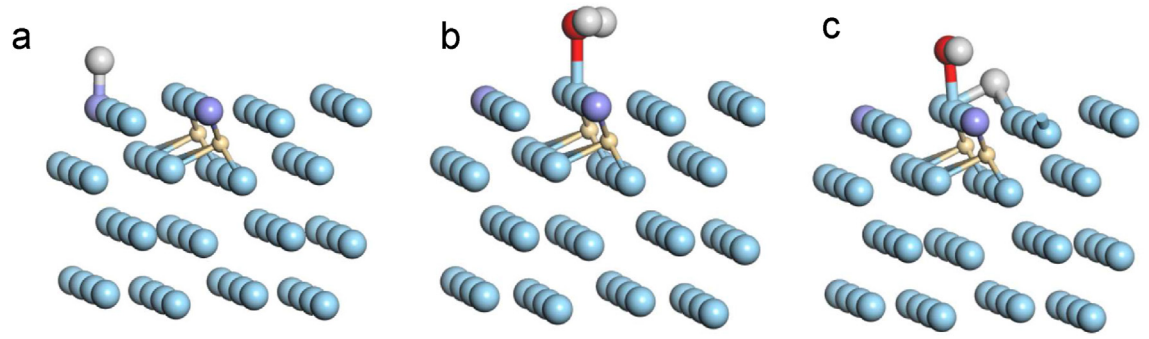

*Fig. 6. The modeling of (Ru-P)#Pt (101) and the adsorption configurations of H_2O, *OH+*H and *H by DFT calculation. (Ru: light blue; Pt: purple; P: dark yellow; O: red; H: grey).*

Table 3. The energetics of H_2O splitting on (Ru-P)#Pt (101) and Ru (101) surface based on the DFT calculation.

Model	ΔE (H_2O) (eV)	ΔE (OH + H) (eV)	ΔE (H) (eV)
(Ru-P)#Pt	−0.59 (Ru)	−4.43 (Ru)	−0.20 (Pt)
Ru	−0.42	−4.41	−0.60

desorption kinetics of H on Pt site. Interestingly, the adsorptions of *OH and *H on Ru and (Ru-P)#Pt are only slightly changed, indicating that the *OH species shall not impede the further adsorption and splitting of H_2O in the next cycle [25].

4. Conclusions

A method was developed for the preparation of (Ru-P)#Pt/C alloy catalyst with the ratio of Pt to Ru being about 14.4%. Based on the XRD and XPS analyses, it is believed that Pt atoms were dispersed into the P-doped Ru nanoparticles surface. By comparing with the P doped solely Ru nanoparticles and the P-doped and Pt-deposited CNTs, it is concluded that the synergy between the P doped Ru sites and Pt sites may significantly increase the water dissociation and hydrogen desorption kinetics, respectively. Furthermore, the (Ru-P)#Pt/C exhibited a η_{10} of 17 mV, a Tafel slope of 27 $mV \cdot dec^{-1}$ and a TOF of 60.4 s^{-1} at 100 mV vs. RHE, outperforming most of the reported Ru-based catalysts. The DFT calculation demonstrates that the doping of P into Ru can enhance the water adsorption and activation, and the Pt site can behave as an excellent site for H desorption. This work highlights the importance of the nonmetal heteroatom doping in Ru for the activation of the water splitting and the synergistic effect of Pt doping as the desorption site for hydrogen evolution, which may shed light on the rational design of Ru-based catalysts for alkaline water splitting and beyond.

Acknowledgements

This work was supported by the CSG Technology Project (No. GDKJXM20198054).

References

[1] Li Y, Luo Z Y, Ge J J, Liu C P, Xing W. Research progress in hydrogen evolution low noble/non-precious metal catalysts of water electrolysis[J]. J. Electrochem., 2018, 24(6): 572−588.
[2] Zhao G Q, Rui K, Dou S X, Sun W P. Heterostructures for electrochemical hydrogen evolution reaction: a review[J]. Adv. Funct. Mater., 2018, 28(43): 1803291.
[3] Zou H H, Li W Q, Song C H, Cao L M, Zhang X F, Zhu X Y, Du Z Y, Zhang J, Zhong S L, He C T. Disclosing the active integration structure and robustness of a pseudo-tri-component electrocatalyst toward alkaline hydrogen evolution[J]. J. Energy Chem., 2022, 72: 210−216.
[4] Wei Y, Soomro R A, Xie X Q, Xu B. Design of efficient electrocatalysts for hydrogen evolution reaction based on 2D MXenes[J]. J. Energy Chem., 2021, 55: 244−255.
[5] Wang X L, Cong Y Y, Qiu C X, Wang S J, Qin J Q, Song Y J. Core-shell structured Ru@PtRu nanoflower electrocatalysts toward alkaline hydrogen evolution reaction[J]. J. Electrochem., 2020, 26(6): 815−824.
[6] Zhang T J, Walsh A G, Yu J H, Zhang P. Single-atom alloy catalysts: structural analysis, electronic properties and catalytic activities[J]. Chem. Soc. Rev., 2021, 50(1): 569−588.
[7] Hannagan R T, Giannakakis G, Flytzani-Stephanopoulos M, Sykes E CH. Single-atom alloy catalysis[J]. Chem. Rev., 2020, 120(21): 12044−12088.
[8] Liu Y, Liu S L, Wang Y, Zhang Q H, Gu L, Zhao S C, Xu D D, Li Y F, Bao J C, Dai Z H. Ru modulation effects in the synthesis of unique rod-like Ni@Ni_2p-Ru heterostructures and their remarkable electrocatalytic hydrogen evolution performance[J]. J. Am. Chem. Soc., 2018, 140(8): 2731−2734.
[9] Mahmood J, Li F, Jung S M, Okyay M S, Ahmad I, Kim S J, Park N, Jeong H Y, Baek J B. An efficient and pH-universal ruthenium-based catalyst for the hydrogen evolution reaction[J]. Nature Nanotech, 2017, 12(5): 441−446.
[10] Wang X S, Zhu Y H, Vasileff A, Jiao Y, Chen S M, Song L, Zheng B, Zheng Y, Qiao S Z. Strain effect in bimetallic electrocatalysts in the hydrogen evolution reaction[J]. ACS Energy Lett., 2018, 3(5): 1198−1204.
[11] Wang C, Qi L M. Heterostructured inter-doped ruthenium-cobalt oxide hollow nanosheet arrays for highly efficient overall water splitting[J]. Angew. Chem. Int. Ed., 2020, 59(39): 17219−17224.
[12] Luo M, Cai J Y, Zou J S, Jiang Z, Wang G M, Kang X W. Promoted alkaline hydrogen evolution by an N-doped Pt-Ru single atom alloy[J]. J. Mater. Chem. A, 2021, 9(26): 14941−14947.
[13] Muleja A A, Mbianda X Y, Krause R W, Pillay K. Synthesis, characterization and thermal decomposition behaviour of

triphenylphosphine-linked multiwalled carbon nanotubes [J]. Carbon, 2012, 50(8): 2741−2751.
[14] Song H Y, Ma C L, Wang L, Zhu Z G. Platinum nanoparticle-deposited multi-walled carbon nanotubes as a NADH oxidase mimic: characterization and applications[J]. Nanoscale, 2020, 12(37): 19284−19292.
[15] Chen C, Kang Y J, Huo Z Y, Zhu Z W, Huang W Y, Xin H LL, Snyder J D, Li D G, Herron J A, Mavrikakis M, Chi M F, More K L, Li Y D, Markovic N M, Somorjai G A, Yang P D, Stamenkovic V R. Highly crystalline multimetallic nanoframes with three-dimensional electrocatalytic surfaces[J]. Science, 2014, 343(6177): 1339−1343.
[16] Xie Y F, Cai J Y, Wu Y S, Zang Y P, Zheng X S, Ye J, Cui P X, Niu S W, Liu Y, Zhu J F, Liu X J, Wang G M, Qian Y T. Boosting water dissociation kinetics on Pt-Ni nanowires by N-induced orbital tuning[J]. Adv. Mater., 2019, 31(16): 1807780.
[17] Zhang Z C, Liu G G, Cui X Y, Chen B, Zhu Y H, Gong Y, Saleem F, Xi S B, Du Y H, Borgna A, Lai Z C, Zhang Q H, Li B, Zong Y, Han Y, Gu L, Zhang H. Crystal phase and architecture engineering of lotus-thalamus-shaped Pt-Ni anisotropic superstructures for highly efficient electrochemical hydrogen evolution[J]. Adv. Mater., 2018, 30(30): 1801741.
[18] Fan J C, Qi K, Zhang L, Zhang H Y, Yu S S, Cui X Q. Engineering Pt/Pd interfacial electronic structures for highly efficient hydrogen evolution and alcohol oxidation[J]. ACS Appl. Mater. Inter., 2017, 9(21): 18008−18014.
[19] Zhao Z P, Liu H T, Gao W P, Xue W, Liu Z Y, Huang J, Pan X Q, Huang Y. Surface-engineered PtNi-O nanostructure with record-high performance for electrocatalytic hydrogen evolution reaction[J]. J. Am. Chem. Soc., 2018, 140(29): 9046−9050.
[20] Cao Z M, Chen Q L, Zhang J W, Li H Q, Jiang Y Q, Shen S Y, Fu G, Lu B A, Xie Z X, Zheng L S. Platinum-nickel alloy excavated nano-multipods with hexagonal close-packed structure and superior activity towards hydrogen evolution reaction[J]. Nat. Commun., 2017, 8: 15131.
[21] Ding J B, Shao Q, Feng Y G, Huang X Q. Ruthenium-nickel sandwiched nanoplates for efficient water splitting electrocatalysis[J]. Nano Energy, 2018, 47: 1−7.
[22] Li K, Li Y, Wang Y M, Ge J J, Liu C P, Xing W. Enhanced electrocatalytic performance for the hydrogen evolution reaction through surface enrichment of platinum nanoclusters alloying with ruthenium *in situ* embedded in carbon[J]. Energy Environ. Sci., 2018, 11(5): 1232−1239.
[23] Wu R, Xiao B, Gao Q, Zheng Y R, Zheng X S, Zhu J F, Gao M R, Yu S H. A janus nickel cobalt phosphide catalyst for high-efficiency neutral-pH water splitting[J]. Angew. Chem. Int. Ed., 2018, 57(47): 15445−15449.
[24] Wan R D, Luo M, Wen J B, Liu S L, Kang X W, Tian Y. Pt-Co single atom alloy catalysts: accelerated water dissociation and hydrogen evolution by strain regulation[J]. J. Energy Chem., 2022, 69: 44−53.
[25] Qin X P, Zhu S Q, Zhang L L, Sun S H, Shao M H. Theoretical studies of metal-N-C for oxygen reduction and hydrogen evolution reactions in acid and alkaline solutions [J]. J. Electrochem., 2021, 27(2): 185−194.

磷掺杂的 Ru-Pt 合金催化剂及其电催化碱性析氢性能

黄荣钦[a]，廖卫平[b]，晏梦璇[b]，刘　石[a]，李远明[a]，康雄武[a,*]
[a]广东慧氢能源科技有限公司，广东 广州 510000
[b]广东电网有限责任公司江门供电局，广东 江门 529000

摘要

可再生能源驱动电催化水分解产氢气在现代氢能及氢燃料电池可持续发展方面，有着极其重要的地位。其中，性能优良催化剂的设计与开发又是重中之重。本文重点发展了一种磷掺杂的铂-钌合催化剂(Ru-P)#Pt/C），TEM 分析确认 Ru 金属纳米粒子的球形形态，XRD 表征 Ru 纳米粒子以六方密堆积形式存在。XPS 分析进一步说明了 Ru 以金属态存在，Pt 的原子比在 14.5%左右，且以轻微氧化的状态存在，表明其可能与 P 成键。(Ru-P)@Pt 合金催化剂在碱性电解液中表现出优异的电解水析氢性能，在 10 mA·cm^{-2} 的电流密度下的过电位仅为 17 mV vs. RHE，Tafel 斜率值为 27 mV·dec^{-1}，表明该催化剂析氢决速步为 Tafel 步骤。而同等条件下，仅 P 掺杂的 Ru 催化剂及 Pt 负载的 P 掺杂的 CNT，其性能均远逊于该目标催化剂，表明了 P 与 Pt 共掺杂的协同作用。(Ru-P)#Pt/C 合金催化剂经过 24 h 耐久性测试，其 10 mA·cm^{-2} 的过电位及稳定性测试后 LSV 电流仅出现轻微衰退。这表明 P 掺杂的 Ru-Pt 合金催化剂中 Ru、Pt、P 活性位点间的协同作用，显著提高了电催化析氢活性与稳定性，为高性能碱性电解水析氢催化剂的设计打开了广阔的前景。

关键词： Ru-Pt 合金；磷掺杂；协同效应；双活性位点；电解水析氢